Power Decoupling Method for Single Phase Differential Buck Converter

Wenli Yao[1], Yi Tang[2], Xiaobin Zhang[1], Xiongfei Wang[3], Poh Chiang Loh[3], and Frede Blaabjerg[3]

[1]School of Automation
Northwestern Polytechnical University
127Youyi West Road, Xi'an, Shaanxi, 710072, P.R.China
ywl0158@mail.nwpu.edu.cn
dgl907@126.com

[2]School of Electrical and Electronic Engineering
Nanyang Technological University
50 Nanyang Avenue
639798 Singarpore
yitang@ntu.edu.sg

[3]Department of Energy Technology
Aalborg University
Pontoppidanstraede 101, Aalborg, 9220 Denmark
xwa@et.aau.dk, pcl@et.aau.dk, fbl@et.aau.dk

***Abstract*-- The well-known inherent second-order ripple power in single phase converters imposes harmonic stress on the dc link, resulting in low efficiency and overheating issues. In order to avoid installing bulky electrolytic capacitors or *LC* filters in the dc-link, this paper presents a differential buck inverter to improve the dc link power quality, and an improved active power decoupling method is proposed to achieve ripple power reduction for both AC-DC and DC-AC conversions. The ripple energy storage is realized by the filter capacitors, which are connected between the output terminal and the negative dc bus. By properly controlling the differential mode voltage of the capacitors, it is possible to transfer desired energy between the DC port and AC port. The common mode voltage is controlled in such a way that the ripple power on the dc side will be reduced. Furthermore, an autonomous reference generation technique is proposed to provide accurate ripple power compensation, and closed-loop controllers are also designed based on small signal models. The effectiveness of this power decoupling method is verified by detailed simulation studies as well as laboratory prototype experimental results.**

***Index Terms*-- Active power decoupling, differential buck converter, power quality, small signal modeling.**

I. INTRODUCTION

The well-known inherent second-order ripple power in single phase converters imposes harmonic stress on the DC link, which may result in low efficiency and overheating issues. For example, in photovoltaic (PV) applications, the ripple power may challenge the accuracy of maximum power point tracking (MPPT) and reduce the energy yield [1]. In fuel-cell applications, the pulsating power may waste fuel consumption and shorten the lifetime of fuel cells [2]. Traditionally, bulky electrolytic capacitors or *LC* filters can be installed in the dc-link as power decoupling elements to buffer the ripple power [3]. However, from lifetime perspective, electrolytic capacitors (several thousand hours) are not ideal candidates to warranty the entire operation period of inverters [4]. To replace them and resolve these issues, active power decoupling methods are more preferred, and the basic principle is to use additional energy storage elements and switches to create a power decoupling circuit, which prevents the inherent second-order ripple power from flowing into the dc link. The energy storage element (film capacitor or inductor) can be installed on either the AC or DC side [5]-[10]. Therefore, only a small dc bus capacitor is needed to filter the remaining high frequency switching noises. As a result, it is possible to replace electrolytic capacitors or *LC* filters with a long-lifetime film capacitor. Unfortunately, all existing active methods have to introduce extra energy storage elements in the system to process the ripple power, and this may inevitably lead to increased component costs as well as system complexity. On the other hand, the performance of power decoupling largely relies on the control references of the capacitor voltage or inductor current, which are unfortunately parameter dependent. Since the power converters may not work in ideal conditions, the circuit parameters may drift with service time and deviate from their rated values. Under these circumstances, the performance of power decoupling will be degraded. In [3], a close-loop control is first applied to AC-DC converters to generate control signals for the decoupling switching leg. However, the attenuation is not very high at 100Hz. In [11], the DC bus ripple voltage is employed to realize the closed-loop control of power decoupling, and a good dynamic response is demonstrated. Nevertheless, the presented circuit may need additional switches for power decoupling, implying increased power losses and implementation cost.

In this paper, an improved active power decoupling method is proposed to achieve ripple power reduction without using addition switches. The main circuit is based on a differential buck converter initially proposed in [12], [13], where the H-bridge of the inverter is treated as two bidirectional buck converters working in the differential mode and common mode. The differential mode is to transfer energy between the DC port and AC port, and the common mode is to realize power decoupling. The filter capacitors on the AC side are used as the storage element and construct the common mode circuit together with the H-bridge and inductors. Since the compensation of ripple power is accomplished by the common mode operation, the differential AC voltage will not be affected. As a result, this circuit does not require a large dc capacitor or a passive *LC* circuit in the dc link. However, like other alternatives, the performance of the differential buck converter largely relies on its common mode command references, which may be inaccurate due to parameter drift. Therefore, it is necessary

to derive the command references in a closed-loop manner without relying on the system parameters.

In order to achieve this, this paper presents an autonomous reference generation method for buck differential converters, and both AC-DC and DC-AC applications are considered. The generated references can then be fed into closed-loop control schemes with both differential and common-mode regulations. The proposed method differs from the one discussed in [14], because it provides more in-depth analysis on the AC-DC operation, closed-loop controller design, and small signal modeling. It is interesting to find that the AC-DC and DC-AC conversions have the same small-signal model, which is helpful to design the control schemes and derive the transfer functions for evaluation of the power decoupling control. Furthermore, an inner inductor current control is employed to provide damping to the common mode, where the plant model is found to be a typical resonant second order system. Finally, the effectiveness of this power decoupling method is verified by detailed simulation studies as well as laboratory prototype experimental results.

II. Operation Principle of the Proposed Power Decoupling Method

A generic representation of the differential buck converter is given in Fig. 1, where two dc-dc converters share the same set of dc terminals on the dc input, but on the ac side, they only share the '–' terminal. It should be mentioned that the dc link capacitor is dashed, because it may not be required if a constant dc voltage source is assumed for the DC-AC conversion. The potentials of the two '+' terminals on the ac side can be different, but not negative. They can also include different ac ripples, which when controlled to have the same frequency ω and magnitude but opposite phases, will result

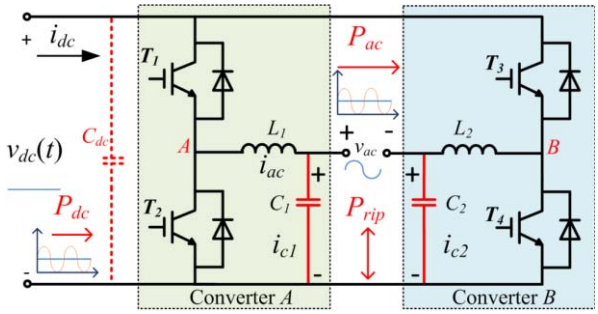

Fig. 1. Schematic of the buck differential converter for power decoupling.

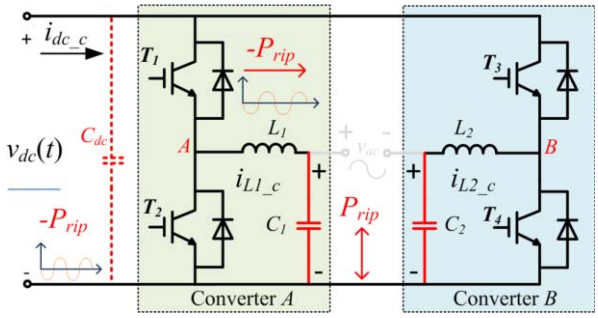

Fig. 2. Equivalent circuit of the buck differential converter in common mode.

in a large differential ac port voltage noted as $v_{ac} = v_{c1} - v_{c2}$ in Fig. 1 (differential mode). In contrast, the dc components of v_{c1} and v_{c2} are controlled to be equal so that they cancel in v_{ac}. The cancellation is not restricted to be dc components, but can also be extended to ac components if they are of the same frequency, magnitude and phase. This cancellation has, in fact, been explored for power ripple decoupling, where v_{c1} and v_{c2} are controlled to have the same ac component at 2ω, where ω is the fundamental angular frequency. Power ripple at 2ω generated by the common ac and dc components will then cancel that from the differential ac component, leading to only constant power flowing through the dc port on the left of Fig. 1. Conventionally, voltage control will be applied on the respective converter to ensure that the capacitor voltage of each converter to be as follows,

$$\begin{cases} v_{c1}(t) = \dfrac{V_{dc}}{2}\left[1 + M_d \sin(\omega t)\right] \\ v_{c2}(t) = \dfrac{V_{dc}}{2}\left[1 - M_d \sin(\omega t)\right] \end{cases} \tag{1}$$

where M_d represents the modulation index, V_{dc} is the DC port average voltage. Thus, the differential voltage of the two capacitors and AC current can be expressed as,

$$\begin{cases} v_{ac}(t) = v_{c1}(t) - v_{c2}(t) = V_m \sin(\omega t) \\ i_{ac}(t) = I_m \sin(\omega t + \varphi) \end{cases} \tag{2}$$

where V_m and I_m are the amplitudes of the output voltage and current, respectively, φ is the phase angle between $v_{ac}(t)$ and $i_{ac}(t)$. The DC power $P_{dc}(t)$ and AC power $P_{ac}(t)$ of the converter are calculated as,

$$\begin{cases} P_{ac}(t) = \dfrac{1}{2} V_m I_m \cos\varphi - \dfrac{1}{2} V_m I_m \cos(2\omega t + \varphi) \\ P_{dc}(t) = v_{dc}(t) \cdot i_{dc}(t) \end{cases} \tag{3}$$

Ignoring the converter loss, $P_{dc}(t) = P_{ac}(t)$. Hence, the 2ω ripple power is transferred to the dc port. Assuming the dc voltage is constant, the output current of the converter can be given as,

$$i_{dc}(t) = \frac{V_m I_m}{2V_{dc}} \cos\varphi - \frac{V_m I_m}{2V_{dc}} \cos(2\omega t + \varphi) \tag{4}$$

Equation (3) shows that the H-bridge converter produces reactive power at 2ω, and this can lead to the ripple component with the same frequency on the DC current. The magnitude of ripple current can be up to the average value of DC current in case of φ=0, as shown in (4). In order to use the AC capacitor as the storage element to compensate this 2ω reactive power, an additional 2ω voltage must be applied to the capacitors, which should work in the common mode so that the ac port voltage expressed in (2) will not be affected. The capacitor voltage after the compensation control can be rewritten as,

$$\begin{cases} v_{c1}(t) = \dfrac{V_{dc}}{2}\left[1 + M_d \sin(\omega t) + M_c \sin(2\omega t + \theta)\right] \\ v_{c2}(t) = \dfrac{V_{dc}}{2}\left[1 - M_d \sin(\omega t) + M_c \sin(2\omega t + \theta)\right] \end{cases} \tag{5}$$

where M_c represents the modulation index in the common mode. In this case, $v_{ac}(t)$ still equals to (2). The common mode capacitor voltage can be given out as,

$$v_{c-com}(t)=\frac{V_{dc}}{2}\left[1+M_c\sin(2\omega t+\theta)\right] \quad (6)$$

Equations (2) and (6) indicate that the differential mode and common mode are operating independently without interaction. Thus, the common mode circuit can be redrawn as in Fig. 2, where its AC side is neglected. The common mode is controlled to work with 2ω frequency, and an opposite 2ω power is generated by the capacitors to compensate the ripple power in the dc link, as shown in (3). By adding such compensating components, it is possible to control v_{c1} and v_{c2} to mitigate the DC ripple power. Thus, for both AC-DC and DC-AC conversions, the common mode dc current $i_{dc\_c}(t)$ can be derived as follows,

$$\begin{aligned} i_{dc\_c}(t)&=\frac{1}{2}\left(i_{L1\_c}(t)+i_{L2\_c}(t)\right)\cdot\left(1+M_c\sin(2\omega t+\theta)\right)\\ &=I_{m\_c}\cos(2\omega t+\theta)\left(1+M_c\sin(2\omega t+\theta)\right) \end{aligned} \quad (7)$$

$$i_{L1\_c}(t)=i_{L2\_c}(t)=I_{m\_c}\cos(2\omega t+\theta) \quad (8)$$

where θ is the common mode phase shift angle with respect to the converter input voltage, $i_{L1\_c}(t)$ and $i_{L2\_c}(t)$ are the inductor currents in the common mode, and their magnitude equals to $\omega C V_{dc} M_d$. Finally, $i_{dc\_c}(t)$ can be expressed as,

$$i_{dc\_c}(t)=I_{m\_c}\cos(2\omega t+\theta)+\frac{1}{2}I_{m\_c}M_c\sin(4\omega t+2\theta) \quad (9)$$

Equation (9) indicates that the common mode dc current can be decomposed into a second order component and a forth order component. The second order term is used to compensate the 2ω ripple current shown in (4), which is caused by the differential mode operation. Unfortunately, for fully compensation of 2ω ripple current, a forth order harmonic has to be introduced in the dc link current with a peak value of $I_{m\_c}*M_c/2$ as shown in (9). Even though $I_{m\_c}*M_c/2$ is much smaller than the 2ω ripple current, it still needs to be fully suppressed. Using a forth order resonant controller in parallel with a proportional resonant (PR) controller can solve this problem, but may further introduce 6ω and 8ω ripple currents. Fortunately, the impacts of high order ripple currents are basically negligible because their amplitudes decrease as the frequency increases.

III. Overall Control Method for AC-DC and DC-AC Conversions

A. AC-DC Rectification

The differential buck converter is shown in Fig. 1, which has an AC source input and an output dc load across a dc capacitor for ac-dc rectification. The differential mode controller is to control the average DC voltage, which can be realized by using the classical dual-loop control structure as shown in Fig. 3. The DC voltage is sensed and filtered by a notch filer (NF), whose notch frequency is tuned at 2ω to obtain the average voltage. The error of the dc average voltage is therefore controlled by a PI controller, giving the reference for the inner current loop. A proportional resonant (PR) controller is employed to improve the performance of current control.

For the common mode operation, its main control objective is to force the 2ω ripple component to be zero, and this ripple component may exist in both the dc output voltage and output current. For simplicity, the capacitor ripple voltage V_{dc_rip} is chosen as the control variable, because it is already measured in the differential mode. The ripple voltage is then regulated to zero by an outer PR controller tuned at 2ω and 4ω. The transfer function of the PR controller is given in (10), where k_p and k_i are the usual controller gains [15].

$$G_{PR}(s)=k_p+\frac{k_i s}{s^2+(2\omega)^2}+\frac{k_i s}{s^2+(4\omega)^2} \quad (10)$$

As mentioned in section II, the 4ω resonant controller is added in order to suppress the corresponding ripple voltage introduced by the 2ω resonant controller. The output of this PR controller will give the reference at 2ω and 4ω for the inner current control. To obtain the ac common mode current, the currents flowing out from the converter through L_1 and L_2 in Fig. 2(a) are sensed and summed together. The inner proportional controller will produce the necessary $M_c\sin(2\omega t+\theta)$ and $M_4\sin(2\omega t+\gamma)$ terms in (5) without knowing the system parameters. Due to the closed-loop control mechanism, the proposed control method is less sensitive to parameter variations and provides more accurate power decoupling.

B. DC-AC Conversion

The inverter remains the same structure as shown in Fig. 1, but has an input dc source and an output ac load. The objective of the differential mode is to control the output ac voltage $v_{ac}(t)$, which is the difference between the two capacitors' voltages, as shown in Fig. 4. A PR controller is adopted to regulate $v_{ac}(t)$ to follow its reference, and an inner inductor current loop is controlled by a simple proportional

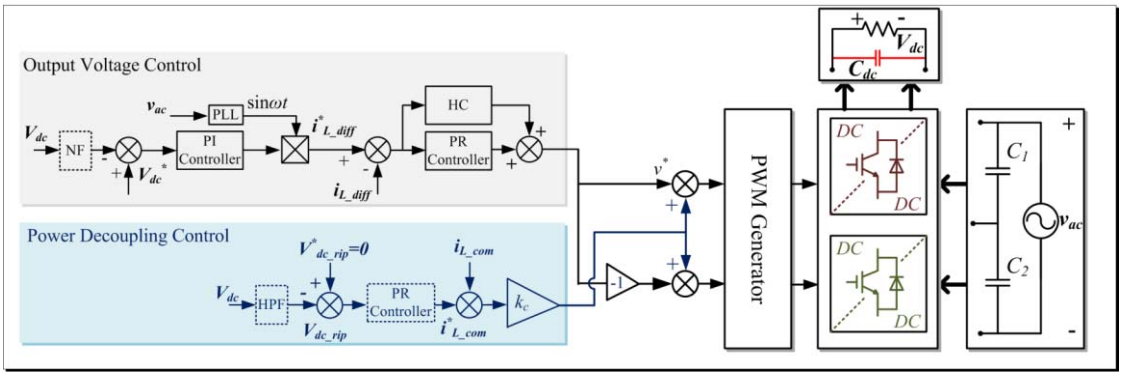

Fig. 3. Control structure of AC-DC rectification.

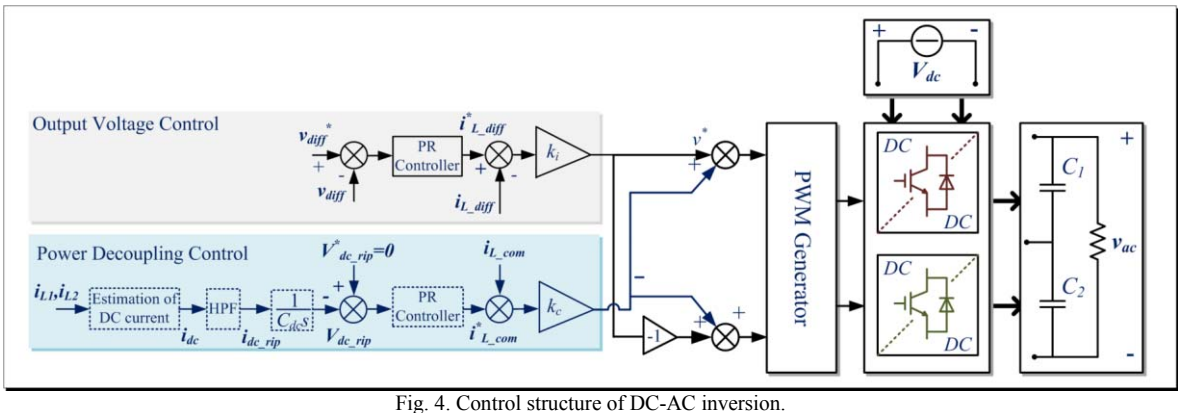

Fig. 4. Control structure of DC-AC inversion.

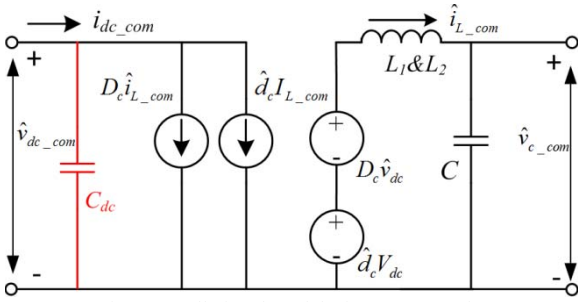

Fig. 5. Small-signal model of common mode.

controller instead of a PR controller. Unlike the rectification case, for the common mode operation, the dc voltage is no longer controllable because of the presence of a stiff dc voltage source. The control variable can only be the dc terminal current, which unfortunately is not continuous but pulsating. Sensing of pulsed current is difficult because it should be synchronized with the converter switching to remove the high frequency components. An alternative way is to compute the dc current from the measured ac currents through L_1 and L_2, and the modulating references for the two buck converters. It should be noted that the modulating references here are the signals directly used for pulse-width modulation (PWM), and are different from those given in (5). Therefore, although explicit power balancing computation is still performed, it only involves the immediate dc and ac power of the converter, and is not affected by the variations of the passive components. The method for estimation of the dc current can be expressed as,

$$i_{dc}(t)=\frac{1}{2}\left[i_{L1}(t)\cdot d_1(t)+i_{L2}(t)\cdot d_2(t)\right] \tag{11}$$

where $d_1(t)$ and $d_2(t)$ are the PWM signals directly used for the DC-DC converters A and B respectively, and denoted as,

$$\begin{cases} d_1(t)=1+M_d\sin(\omega t)+M_c\sin(2\omega t+\theta)+M_4\sin(4\omega t+\gamma) \\ d_2(t)=1-M_d\sin(\omega t)+M_c\sin(2\omega t+\theta)+M_4\sin(4\omega t+\gamma) \end{cases} \tag{12}$$

The 2ω ripple current i_{dc_rip} is extracted from the computed dc current i_{dc}. To keep AC-DC and DC-AC conversions have the same common mode control structure, i_{dc_rip} must be integrated by $1/(sC_{dc})$, where C_{dc} is an arbitrarily chosen capacitance whose value is simply part of the gain required along the control path. To some extent, the integration essentially converts the 2ω ripple current into a virtual 2ω ripple voltage, which then can be used with the dual voltage-current control discussed in the AC-DC conversion section.

IV. Small-Signal Modeling of the Common Mode and Controller Design

As explained before, a differential converter has two operating modes, i.e. differential mode and common mode. The former is for power transfer between the ac and dc sides, and is related to $\pm M_d\sin(2\omega t)$ in (5). On the other hand, the latter is for power decoupling, and is related to $M_c\sin(2\omega t+\theta)$ and $M_4\sin(4\omega t+\gamma)$ in (5). The differential small-signal model is out of view in this paper, as it is already detailed in [16]. The common mode can be derived from small-signal models typically used with dc-dc converters, for both AC-DC and DC-AC conversions, as shown in Fig. 5 [12].

A. Small-Signal model of the common mode

As explained before, the fundamental of power decoupling is to build up a common mode voltage on the filter capacitors, and their induced 2ω ripple power can then be used to compensate the ripple power in the dc port. Therefore, even though AC-DC and DC-AC conversions have different power flow, their equivalent common mode circuit is the same and can be simply treated as a buck converter. The small-signal model under the common mode can be derived by using the PWM switching modeling method in [17] and depicted in Fig. 5. It should be mentioned that the dc port capacitor is highlighted in Fig. 5, as its ripple voltage is the chosen as the control variable for both conversions. For AC-DC conversion, a small capacitor is installed in the dc port to attenuate the switching harmonics. However, in order to obtain the transfer function from duty ratio to output, the dc port capacitor is bypassed and will not be reflected in the transfer function. Thus, the transfer function from duty ratio to common mode dc ripple voltage can be derived and expressed in (13) for both AC-DC and DC-AC conversions.

$$\frac{\hat{v}_{dc\_com}(s)}{\hat{d}_c(s)}=\frac{\left(LCs^2+1\right)I_{L\_com}+D_cV_{dc}C\cdot s}{\left(LC\cdot s^2+1\right)\cdot C_{dc}\cdot s} \tag{13}$$

where I_{L_com} and D_c are the common mode average inductor current and duty ratio respectively. The Bode plot of (13) is drawn in Fig. 7 using the parameters shown in Table I.

TABLE I PARAMETER OF THE INVERTER

Nominal Power	P_n	1 kW
Switching frequency	f_{sw}	20 kHz
Line frequency	f_n	50 Hz
Dc-link voltage	V_{dc}	450 V
Filter inductor	L_1/L_2	1 mH
Filter capacitor	C_1/C_2	60 μF
Nominal load	R_L	200 Ω
Output voltage (rms)	V_{ac}	220 V

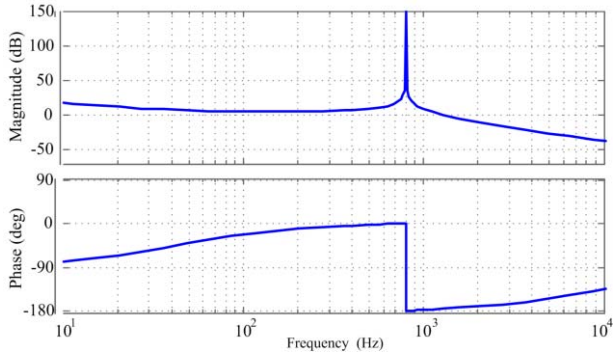

Fig. 7. Bode plot of the transfer function from duty ratio to common mode dc ripple voltage.

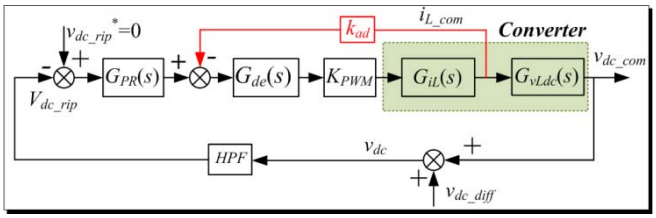

Fig. 8. Control structure of common mode.

Obviously, a resonant phenomenon can be observed at the resonant frequency ω_{res} with a -180° phase change, where ω_{res} is denoted as,

$$\omega_{res} = \sqrt{\frac{1}{LC}} \tag{14}$$

Such a resonance peak may make the entire system unstable, and impose an increasing challenge to the common controller design if the PWM calculation and sampling delay is considered in control.

B. Controller design of common mode

As described in section III, the dc ripple voltage v_{dc_rip} is chosen as the control variable for both conversions, and it is extracted from the dc voltage by a high pass filter. For AC-DC conversion, the ripple voltage can be easily obtained because the dc voltage is already measured. For DC-AC conversion, an integrator $1/(sC_{dc})$ is employed to convert the dc ripple current into ripple voltage. The dc voltage can be treated as the sum of the common mode and differential mode dc voltage v_{dc_com} and v_{dc_diff} respectively. When only the common control is considered, the differential mode dc voltage v_{dc_diff} can be viewed as disturbance. Fig. 8 shows the control structure for the common mode, where $G_{PR}(s)$ is the PR controller mentioned in (10), and $G_{de}(s)$ represents the system delay $e^{-1.5Ts}$ and can be expressed by,

$$G_{de}(s) = \frac{1}{1.5T_s \cdot s + 1} \tag{15}$$

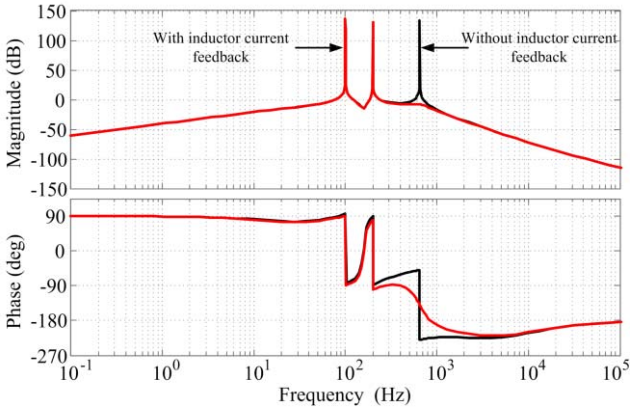

Fig. 9. Bode plot of open loop (with/without inductor current feedback).

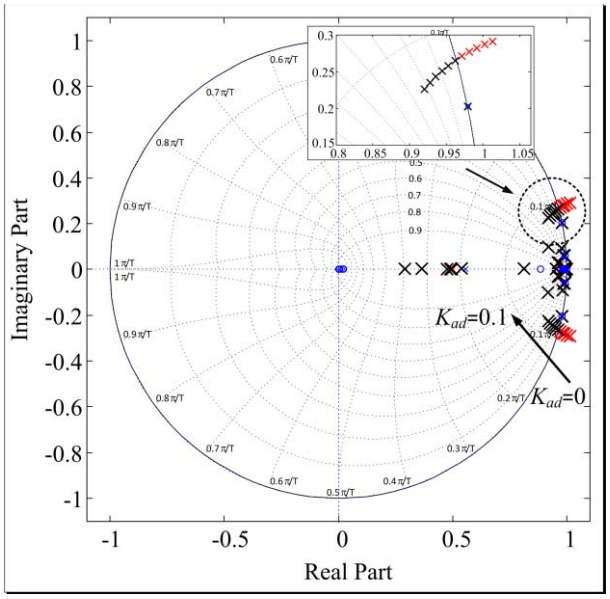

Fig. 10. Zero and pole plot of common mode with difference inductor current feedback gain K_{ad}.

where T_s is the sampling time. $G_{iL}(s)$ is the transfer function from duty ratio to inductor current, which also can be derived from the small-signal model and expressed as (16).

$$G_{iL\_com}(s) = \frac{\hat{i}_{L\_com}}{\hat{d}_c} = \frac{C \cdot s}{LC \cdot s^2 + 1} \tag{16}$$

$G_{vLdc}(s)$ is related to the common-mode inductor current to the dc terminal current according to (17), which mathematically, can be determined by dividing (13) from (16).

$$G_{vLdc}(s) = \frac{G_{vdc\_com}(s)}{G_{iL\_com}(s)} \tag{17}$$

Thus, the open-loop transfer function of the common mode can be derived as (18).

$$G_{open}(s) = K_{PWM} \cdot G_{PR}(s) \cdot G_{de}(s) \cdot G_{vdc}(s) \cdot G_{HPF}(s) \tag{18}$$

Substituting all functions into (18) then allows its Bode diagram to be plotted in Fig. 9 by using the parameters in Table I. The gains of PR controller are calculated according to the technical optimum criterion [18],

$$k_p = \frac{C_{dc}}{\alpha \cdot 4T_s} \tag{19}$$

where α is determined by the desired crossover frequency ω_c and phase margin ψ, which are related as follows,

$$\begin{cases} \alpha = \dfrac{1+\cos\psi}{\sin\psi} \\ \omega_c = \dfrac{1}{\alpha \cdot 4T_s} \end{cases} \tag{20}$$

It should be pointed out that the resonant peak of the *LC* makes its phase response cross the -180° line, indicating an unstable system according to Nyquist criteria. In order to remove the resonant peak, the common mode inductor current is employed to create an inner current loop to damp the resonance via a feedback gain K_{ad} as highlighted in Fig. 8. Thus, a damping term $K_{ad}K_{PWM}Cs$ is added into $G_{vdc}(s)$ as shown in (13). This is similar to the virtual resistor active damping used in the *LCL* filter control [19]. After introducing the inner current loop, the open loop Bode diagram can be re-plotted in Fig. 9, where the resonant peak is successfully suppressed, and there is no -180° phase crossing above 0 dB. This demonstrates that the inner current loop can attract the resonance poles into stable regions. The pole zero maps of the common mode system with different inductor feedback gains ($0<K_{ad}<0.1$) are shown in Fig. 10, where it is clear that as the damping gain K_{ad} increases, the unstable poles are moved into the unit circle, resulting in a stable system.

V. Simulation and Experimental Result

Simulation and experimental systems have been tested to verify the controller performance. The system parameters are given in Table I. The simulation study for the proposed power decoupling method was done under ideal conditions with inductor resistance neglected. Hence, simulation can be considered to represent the worst working condition because there is no passive damping. Simulations were performed with PLECS using a single-phase differential buck converter feeding a resistive load. The experimental system (see Fig. 11) consisted of a 1 kW single-phase prototype connected to an ac source through inductors L_1, L_2 and capacitors C_1, C_2. A Dspace 1006 control board was used for execution of the control algorithms and PWM waveform generation. Fig. 12(a)-(d) show the simulation results, where the differential converter was operating at rated power with a pure resistive load. The waveforms of the capacitor voltages (v_{c1}, v_{c2}), ac source voltage (v_{ac}) and dc output voltage (v_{dc}), without power decoupling control and with power decoupling control are shown in Fig. 12 (a) and (b) respectively. The capacitor voltage contains a third order distortion when the power decoupling is disabled. This is because the second order ripple voltage in the dc voltage cannot be completely removed by the notch filter. When the power decoupling is enabled, a second order distortion may appear in the capacitor voltage instead of the third one. It is clear that with the proposed power decoupling method, the second order voltage ripple in the input is successfully mitigated as compared to the 70V peak-to-peak ripple

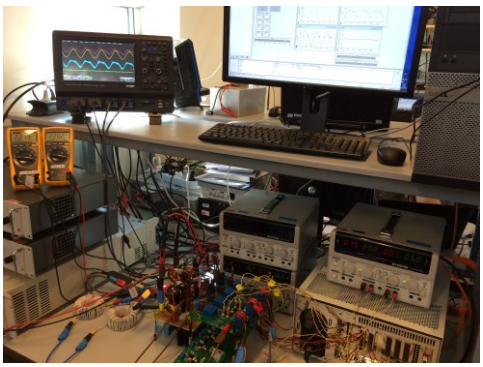

Fig. 11. Laboratory setup of differential converter.

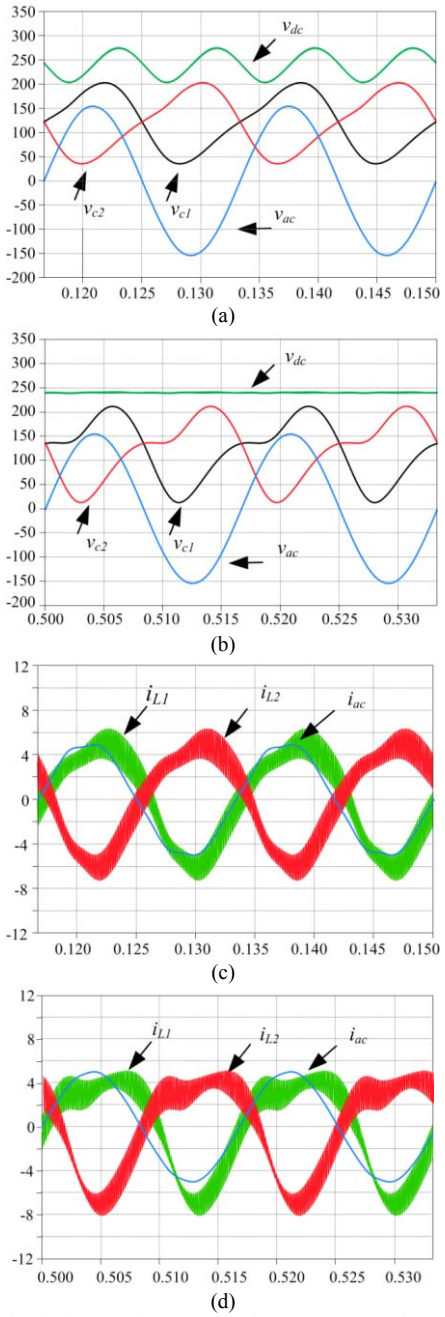

Fig. 12. Simulation result: Output voltage (v_{dc}), ac voltage (v_{ac}) and capacitor voltage (v_{c1},v_{c2}) (a):without decoupling; (b):with decoupling. Inductor current (i_{L1},i_{L2}), ac input current (i_{ac}) (c) :without decoupling; (d):with decoupling .

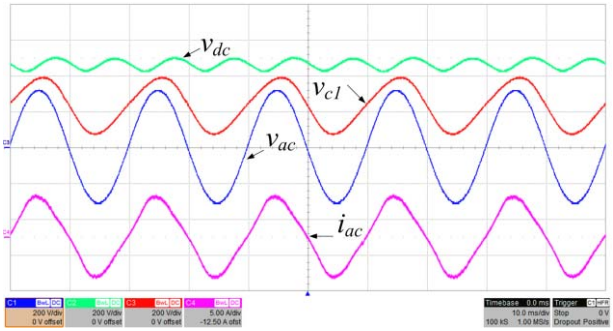

(a)

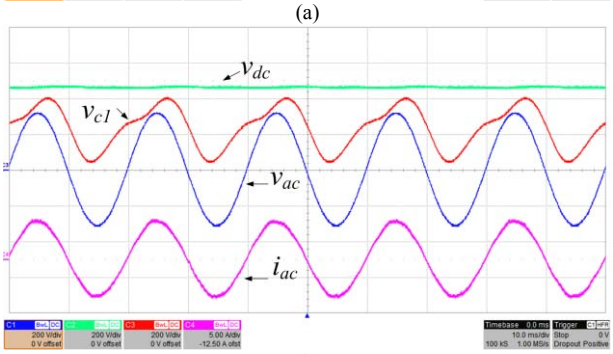

(b)

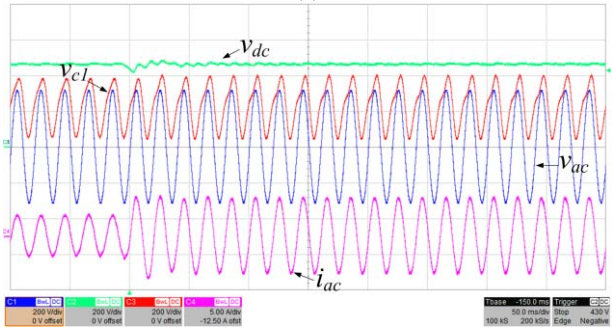

(c)

Fig. 13. Experimental result of AC-DC rectification: (a): without decoupling; (b): with decoupling; (c) the transient performance of 50% to 100% step-up load change. dc output voltage (v_{dc}: 200V/div), capacitor voltage (v_{c1}: 200V/div), inductor current (i_{L1}: 5A/div), and ac source voltage (v_{ac}: 200V/div).

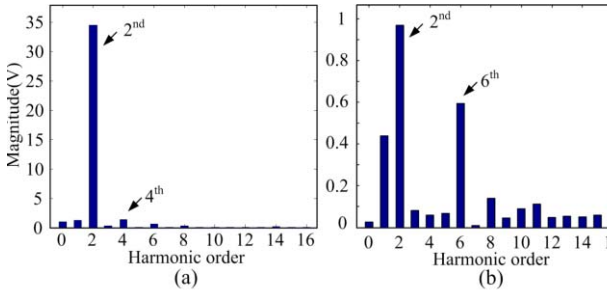

Fig. 14. Spectra of the output voltage v_{dc} in AC-DC rectification: (a) without decoupling; (b) with decoupling.

voltage observed in Fig. 12(a) without power decoupling. Fig. 12(c) and (d) respectively show the waveforms of the inductor current (i_{L1},i_{L2}) and the input current of the inverter (i_{ac}), without power decoupling control and with power decoupling control. The ac input current becomes sinusoidal with much less 3rd distortion when the power decoupling is enabled. Fig. 13 shows the steady-state experimental results of the proposed decoupling method. It is clear that the

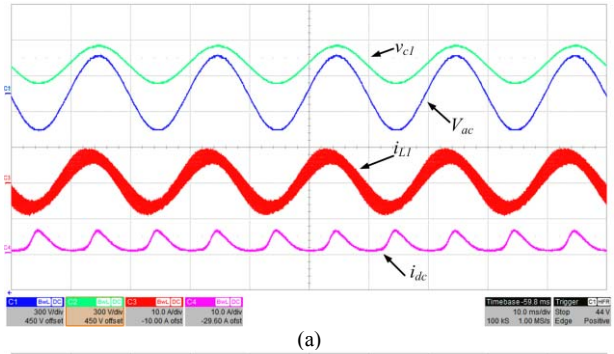

(a)

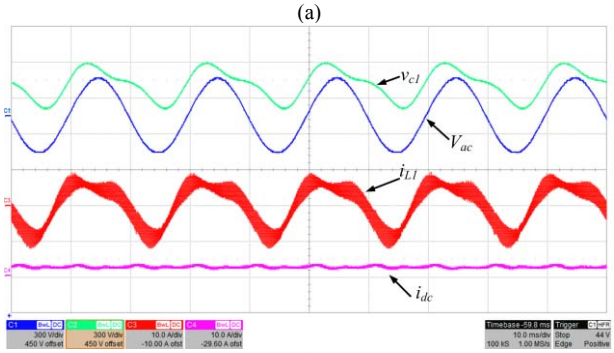

(b)

Fig. 15. Experimental result of DC-AC inversion: dc input current (i_{dc}: 10A/div), capacitor voltage (v_{c1}: 300V/div), inductor current (i_{L1}: 10A/div) and output voltage (v_{ac}: 300V/div) (a): without decoupling; (b): with

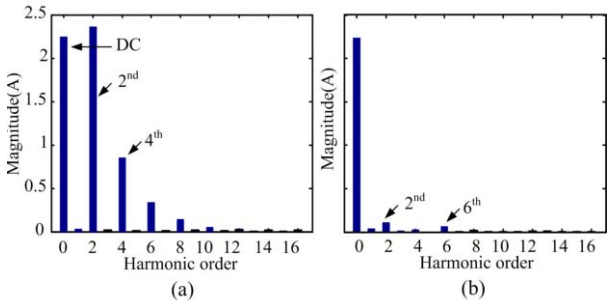

Fig. 16. Spectra of the input voltage i_{dc} in DC-AC inversion: (a) without decoupling; (b) with decoupling.

dc-link voltage ripple can be dramatically reduced as shown in Fig. 13(a) and (b), and the input ac current i_{ac} is sinusoidal with power decoupling. The spectrum of the ripple voltage v_{dc_rip} is shown in Fig. 14, with the power decoupling control, the 2nd ripple voltage is substantially suppressed from 35V down to 1V. It also can be seen that very small fundamental and 6th components still exist when the active decoupling is enabled. This is due to the interactions between the modulation signals (2ω and 4ω) and the common mode harmonic current introduced by (12), which is explained in section III. Using a 6th resonant controller can mitigate the 6th harmonic, but this may burden the DSPACE calculation. The converter was also tested with dynamic loads and the corresponding load step-up experimental results are presented in Fig. 13 (c). The dc-link voltage dip during load transients can be kept within 60V. This is acceptable considering the very low equivalent dc-link capacitance used in the converter. It is obvious that with the proposed decoupling control, the dc output voltage will be very smooth and the negative effects of the ripple voltage can be completely eliminated.

The power decoupling was also tested for the DC-AC conversion based on the same parameters listed in Table I. A 450V dc source was used instead of the dc load. Unlike the AC-DC case where the ripple voltage is measured, the control variable in this case was obtained from the integrator, whose input is the dc current. The measured ac currents through L_1 and L_2, and the modulating references for the two buck converters are employed to compute the dc current for the intention of saving a current sensor. Fig. 15 shows the experimental result of the buck differential converter working under the DC-AC conversion mode. The capacitor voltage contains a second order distortion with power decoupling. Consequently, the peak-to-peak value of the ripple dc current is drmasticcally reduced with the ac output voltage being kept as sinusodal. The spectrum of the input current i_{dc} is also shown in Fig. 16, with the power decoupling control, the 2nd ripple current is suppressed obviously. It also can be seen that the 6th is slightly increased when active decoupling is enabled. This is due to the interaction between 2ω modulation signal and 4th harmonic current introduced by (9).

VI. Conclusion

This paper presents the power decoupling method of differential buck converters for both AC-DC and DC-AC applications. The common mode circuit is employed to compensate the second order ripple power induced by the differential mode operation. In order to make the power decoupling less dependent to the system parameters, an autonomous reference generation technique is proposed for the common mode control. This is realized by forcing the dc link ripple voltage to zero, and then a common mode capacitor voltage control signal is produced. Furthermore, the small signal model is analyzed to derive the common mode transfer functions for both conversions. An inner inductor current control loop is embedded to provide damping effect to stabilize the ripple voltage control, which is originally unstable according to Nyquist criterion. Experimental tests of the converter have been done for both cases, and smooth dc voltage/current as well as high quality ac voltage/current can be obtained with power decoupling. These results successfully prove the effectiveness of the proposed autonomous reference generation techniques and closed-loop control schemes.

References

[1] B. N. Singh, A. Chandra, K. Al-Haddad, A. Pandey, and D. P. Kothari, "A review of single-phase improved power quality AC-DC converters," *IEEE Trans. Ind. Electron*., vol. 50, no. 5, pp. 962-981, Oct. 2003

[2] G-R. Zhu, S-C. Tan, Y. Chen, and C. K. Tse, "Mitigation of low-frequency current ripple in fuel-cell inverter systems through waveform control," *IEEE Trans. Power Electron*., vol. 28, no. 2, pp. 779-792, Feb. 2013.

[3] T. Shimizu, Y. Jin, and G. Kimura, "DC ripple current reduction on a single-phase PWM voltage-source rectifier," *IEEE Trans. Ind. Appl*.,vol. 36, no. 5, pp. 1419-1429, Sep./Oct. 2000.

[4] P. T. Krein, R. S. Balog, and M. Mirjafari, "Minimum energy and capacitance requirements for single-phase inverters and rectifiers using a ripple port*," IEEE Trans. Power Electron*., vol. 27, no. 11, pp. 4690-4698, Nov. 2012.

[5] W. Qi, H. Wang, X. Tan, G. Wang, and K. D. T. Ngo, "A novel active power decoupling single-phase PWM rectifier topology," in *Proc. of IEEE APEC 2014*, pp. 89-95, Mar. 2014.

[6] M. Su, X. Long, Y. Sun, and J. Yang, "An active power decoupling method for single-phase AC/DC converters," *IEEE Trans. Ind. Informat*., vol. 10, no. 1, pp. 461-468, Jan. 2014.

[7] H. Li, K. Zhang, H. Zhao, S. Fan, and J. Xiong, "Active power decoupling for high-power single-phase PWM rectifiers," *IEEE Trans. Power Electron*., vol. 28, no. 3, pp. 1308-1319, Mar. 2013.

[8] H. Wang, H. S. H. Chung, and W. Liu, "Use of a series voltage compensator for reduction of the DC-Link capacitance in a Capacitor-supported system," *IEEE Trans. Power Electron*., vol. 29, no. 3, pp. 1163-1175, Mar. 2014.

[9] R. Wang, F. Wang, D. Boroyevich, and P. Ning, "A high power density single-phase PWM rectifier with active ripple energy storage," *IEEE Trans. Power Electron*., vol. 26, no. 5, pp. 1378-1383, May 2011.

[10] W. Chen and S. Hui, "Elimination of an electrolytic capacitor in ac/dc light emitting diode (LED) driver with high input power factor and constant output current," *IEEE Trans. Power Electron*., vol. 27, no. 3, pp. 1598-1607, Mar. 2012.

[11] Y. Tang, Z. Qin, F. Blaabjerg, and P. C. Loh, "A Dual Voltage Control Strategy for Single-Phase PWM Converters with Power Decoupling Function" in *Proc. of ECCE 2014*, pp.4102-4109, Sep. 2014.

[12] N. Vázquez, J. Almazan, J. Álvarez, C. Aguilar, and J. Arau, "Analysis and experimental study of the buck, boost and buck-boost inverters," in *Proc. of IEEE PESC'99*, pp.801-806, Jun. 1999.

[13] I. Serban, "A novel transistor-less power decoupling solution for single-phase inverters," in *Proc. of IECON 2013*, pp. 1496-1500, Nov. 2013.

[14] I. Serban, " Power Decoupling Method for Single-Phase H-bridge Inverters with no Additional Power Electronics," *IEEE Trans. Ind. Electron*., in press.

[15] R. Teodorescu, F. Blaabjerg, M. Liserre, and P. C. Loh, "Proportional resonant controllers and filters for grid connected voltage source converters," *Proc. Inst. Elect. Eng.-Elect. Power Appl*., vol. 153, no. 5, pp. 750-762, Sep. 2006.

[16] P. Sanchis, A. Ursua, E. Gubia, and L. Marroyo, "Boost DC-AC inverter: A new control strategy," *IEEE Trans. Power Electron.*, vol. 20, no. 2, pp. 343-353, Mar. 2005.

[17] V. Vorperian, "Simplified analysis of PWM converters using model of PWM switch-Part I: Continuous conduction mode," *IEEE Trans. Aerospace Electron. Syst*., vol. 26, pp. 490-496, May 1990.

[18] V. Blasko and V. Kaura, "A new mathematical model and control of a three-phase AC-DC voltage source converter," *IEEE Trans. Power Electron*., vol. 12, no. 1, pp. 116-123, Jan. 1997.

[19] R. Pena Alzola, M. Liserre, F. Blaabjerg, R. Sebastian, J. Dannehl, and F.W. Fuchs, "Systematic design of the lead-lag network method for active damping in *LCL*-filter based three phase converters," *IEEE Trans. Ind. Inf.*, vol. 10, no. 1, pp. 43-52, Feb. 2014.